Description of PEM Fuel Cells System

Diego Feroldi and Marta Basualdo

Abstract This chapter provides a description of polymer electrolyte membrane (PEM) fuel cell-based systems and different modeling approaches. First, it shows the structure of a single cell, the advantages and disadvantages of this type of fuel cell, the expressions of the generated voltage and the efficiency, and the generic structure of a generation system based on PEM fuel cell. Second, the chapter provides a review of the principal models presented in the literature to describe the behavior of the system. Different types of PEM fuel cell models are presented, focusing on dynamic models suitable for control purposes. Particularly, this chapter describes in detail the dynamic model used as a base to represent the system in the subsequent chapters of the book. Then, the described model is used to study the optimal operation of a fuel cell at different loads, showing the benefits of an optimal operation in terms of hydrogen reduction and greater peak power.

1 Introduction

The polymer electrolyte membrane fuel cell (PEMFC), also known as proton exchange membrane fuel cell, takes its name from the type of electrolyte: a polymeric membrane with high proton conductivity when the membrane is conveniently

D. Feroldi (✉) · M. S. Basualdo
CAPEG-CIFASIS-(CONICET-UNR-UPCAM),
27 de Febrero 210 bis, S2000EZP Rosario, Argentina
e-mail: feroldi@cifasis-conicet.gov.ar

M. S. Basualdo
UTN-FRRo, Zeballos 1341, S2000BQA Rosario, Argentina
e-mail: basualdo@cifasis-conicet.gov.ar

D. Feroldi
DCC-FCEIA-UNR, Pellegrini 250, S2000BTP Rosario, Argentina

M. S. Basualdo et al. (eds.), *PEM Fuel Cells with Bio-Ethanol Processor Systems*,
Green Energy and Technology, DOI: 10.1007/978-1-84996-184-4_2,

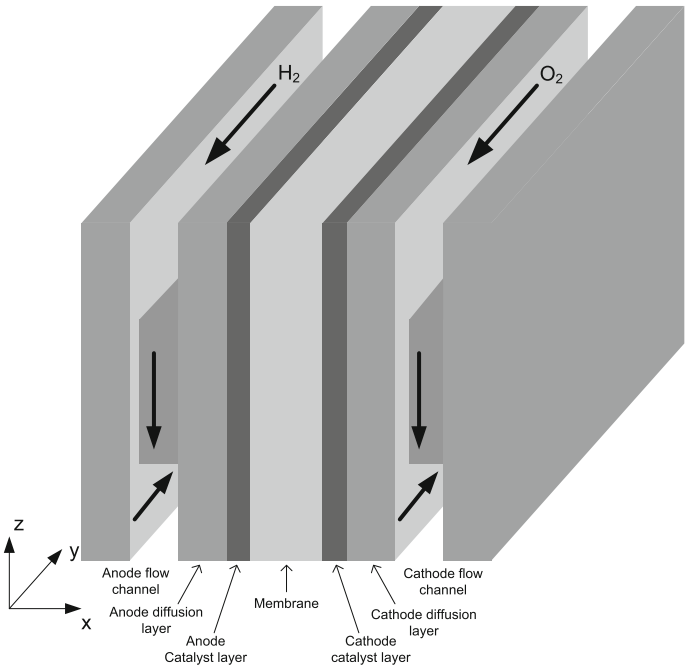

Fig. 1 Three-dimensional schematic diagram of a fuel cell

hydrated [1]. At the moment, the most common polymer used in these types of cells is the Nafion developed by *Du Pont* (USA), which is fabricated with chemically stabilized perfluorosulfonic acid copolymer [2].

1.1 Basic PEM Fuel Cell Structure

Basically, the physical structure of a PEMFC consists of seven components, according to Fig. 1 [3]: feeding channels, diffusion layer, and catalytic layer in the anode; membrane; catalytic layer, diffusion layer, and feeding channels in the cathode. The PEMFC combines in a very compact unit the electrodes and the electrolyte. This structure, well known as membrane electrode assembly (MEA), is not thicker than a few hundred microns. It is the heart of the fuel cell and is fed with hydrogen and oxygen,[1] generating electrical power with a power density of around $1\,\mathrm{W\,cm^{-2}}$ [5].

The polymeric solid electrolyte forms a thin electronic insulator and a barrier for gases between both electrodes, allowing fast proton transport and high current

[1] Usually, the fuel cell is fed with atmospheric air instead of pure oxygen. The oxygen mole fraction in atmospheric air is 0.21 [4].

density. The solid electrolyte has the advantage, as opposed to those of liquid type, that allows the FC to operate in any spatial position [1].

The electrodes consist of a catalytic layer of great superficial area on a substratum of coal, permeable to gases. Electrocatalyst materials are necessary to obtain a good operation, increasing the speed of the chemical reaction. In this way, the gases can react with a lower energy of activation, allowing the reaction to take place at a lower temperature [3]. The electrocatalyst used in PEMFC is platinum, which is one of the major drawbacks of this technology because of its high cost.

However, there are research advances of high temperature PEM fuel cells (HT-PEMFCs) in several fields because there are several reasons for operating at temperatures above 100°C [6]. First, the electrochemical kinetics for the reactions in cathode and anode are enhanced. Second, the water management issue can be simplified because there would be no liquid water. Third, the cooling system is simplified due to the increased temperature gradient between the fuel cell stack and the coolant. Fourth, the waste heat can be exploited using cogeneration. Fifth, the tolerance to CO is increased allowing the use of lower quality reformed hydrogen. Unfortunately, the area of HT-PEMFCs is incipient and still needs much research to be implemented in commercial applications.

1.2 Advantages and Disadvantages of PEM Fuel Cells

The main advantage of PEM fuel cells is their high efficiency compared with other energy conversion devices [7]. This allows the efficiency of a fuel cell vehicle using direct-hydrogen FC[2] to be twice that in a gasoline vehicle [8, 9]. Moreover, unlike the internal combustion engines where the efficiency is maximum with the highest loads, the FC efficiency is also high with partial loads. This is advantageous because in typical driving conditions, like urban and suburban scenarios, most of the time the vehicle is demanding a small fraction of the nominal FC power [10]. Thus, an FC vehicle will be working mostly at high efficiencies. At the same time, using direct-hydrogen FC, the local emissions problem in densely urban areas can be eliminated.

Another important advantage of PEMFC, in contrast to other types of fuel cells, is the low operation temperature (below 80°C) [11], allowing to reach the operation point quickly. In addition, the cost of the materials is smaller than for the high temperature fuel cells (except the catalyst, which is based on platinum) and their operation is safer. All these characteristics turn PEMFC particularly appropriate for applications in vehicles. Nevertheless, it is necessary to use better, and more economic, catalyst so that the reaction occurs at lower temperatures.

The main disadvantage of fuel cells is their high cost and the high production cost of hydrogen. Hydrogen is preferred because of the fast electrochemical reaction, and

[2] Direct-hydrogen FC refers to an FCS that is directly fed with hydrogen from a pressurized tank opposite to the case where the hydrogen is produced with an on-site reformer.

its high specific energy.[3] Nevertheless, as it was mentioned, hydrogen is not a primary fuel. Usually, it is produced from hydrocarbon reforming or water electrolysis [1, 13]. The use of electrolysis is advisable especially when some type of renewable energy is used, avoiding fossil fuel use. It is expected that the cost of fuel cells and hydrogen will diminish with the progress in technology. Thus, hydrogen has the possibilities of becoming an alternative to fossil fuels with the joint use of renewable energies.

1.3 Fuel Cell Voltage

The standard potential E^0 is a quantitative measurement of the maximum cell potential, i.e., the open circuit voltage. For a hydrogen–oxygen cell, in which there is a transfer of two electrons by each water molecule, $E^0 = 1.229\,\text{V}$ if the produced water is in liquid state and $E^0 = 1.18\,\text{V}$ if the produced water is in gaseous state [13]. These values correspond to normalized conditions: cell temperature (T_{fc}) equal to 298.5 K and partial pressures of oxygen (p_{O_2}) and hydrogen (p_{H_2}) equal to 1 atm. In the work of Amphlett et al. [14], the following expression of E^0 is given, depending on the temperature and the reactant partial pressures, which are used in several models of fuel cells e.g., [4, 15]:

$$E^0 = 1.229 - 8.5 \times 10^{-4}\,(T_{\text{fc}} - 298.5) + 4.3085 \times 10^{-5} T_{\text{fc}} \left[\ln\left(p_{\text{H}_2}\right) + \frac{1}{2}\ln\left(p_{O_2}\right) \right]. \tag{1}$$

However, in practice the cell potential is significantly lower than the theoretical potential because there are some losses even when no external load is connected. Moreover, when a load is connected to the fuel cell, the voltage in the terminals decreases still more due to a number of factors, including polarization losses and interconnection losses between cells. The main voltage losses in a fuel cell are the following [1, 13, 16]:

Activation loss The *activation losses* v_{act} are caused by the slowness of the reaction that takes place on the surface of the electrodes. A proportion of the generated voltage is lost in maintaining the chemical reaction that transfers electrons from the negative electrode toward the positive electrode. This phenomenon is strongly nonlinear, and more important, it is at low current densities.

Fuel crossover and internal currents These *energy losses* result from the waste of fuel passing through the electroslyte and from electron conduction through the electrolyte. In PEMFC, the fuel losses and internal current are small and their effects are usually negligible.

[3] The Specific Energy of hydrogen at ambient pressure is $8890\,\text{W h kg}^{-1}$, meanwhile the corresponding one of petrol is $694\,\text{W h kg}^{-1}$. However, the necessary volume for its storage is greater. The energy density of petrol is $500\,\text{W h dm}^{-3}$, meanwhile for hydrogen (300 bar) is $55\,\text{W h dm}^{-3}$ [12].

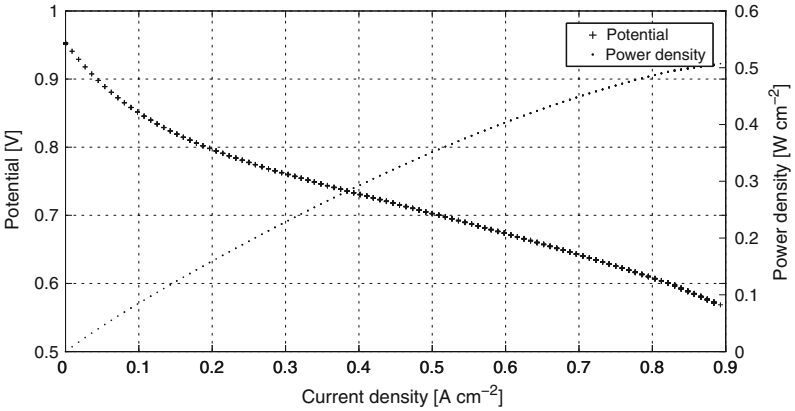

Fig. 2 Polarization curve showing the cell potential and the power density versus the cell current density at $p_{H_2} = p_{O_2} = 2.28$ atm and $T_{fc} = 353$ K

Ohmic loss The *ohmic losses* v_{ohm} are caused by the resistance to the transport of electrons through the electrodes and the different interconnections, and also to the passage of ions through the electrolyte. The behavior of v_{ohm} is approximately linear with the current density.

Concentration loss The *concentration losses* v_{conc} are caused by the diffusion of ions through the electrolyte which produces an increase in the concentration gradient, diminishing the speed of transport. The relation between the voltage of the cell and the current density is approximately linear upto a limit value, beyond which the losses grow quickly.

Therefore, the fuel cell voltage of a simple cell can be expressed as

$$v_{fc} = E^0 - v_{ohm} - v_{act} - v_{conc}. \tag{2}$$

A typical polarization curve showing the potential and power density as a function of the current density is shown in Fig. 2. This curve is obtained using the fuel cell model developed in [4]. In practice, a succession of cells are connected in series in order to provide the necessary voltage and power output, constituting a Fuel Cell Stack System.

1.4 Theoretical and Real Fuel Cell Efficiency

The efficiency of any energy conversion device is defined as the ratio between the useful energy output and the energy input. In a fuel cell, the useful energy output is the generated electrical energy and the energy input is the energy content in the mass of hydrogen supplied. The energy content of an energy carrier is called the Higher Heating Value (ΔH_{HHV}). The ΔH_{HHV} of hydrogen is 286.02 kJ mol^{-1} or 141.9 MJ kg^{-1}. This is the amount of heat that may be generated by a complete combustion of 1 mol or 1 kg of hydrogen, respectively. The ΔH_{HHV} of hydrogen is experimentally

determined by reacting a stoichiometric mixture of hydrogen and oxygen in a steel container at 25°C. If hydrogen and oxygen are combined, water vapor emerges at high temperatures. Then, the container and its content are cooled down to the original 25°C and the ΔH_{HHV} is determined by measuring the heat released between the identical initial and final temperatures. On the contrary, if the cooling is stopped at 150°C, the reaction heat is only partially recovered (241.98 kJ mol^{-1}or 120.1 MJ kg^{-1}). This is known as the *lower heating value* (ΔH_{LHV}) of hydrogen [17].

Assuming that all the Gibbs free energy of hydrogen,[4] ΔG, can be converted into electrical energy, the maximum possible (theoretical) efficiency of a fuel cell is [16]

$$\eta_{\text{HHV}} = -\Delta G/ - \Delta H_{\text{HHV}} = 237.34/286.02 = 83\%. \tag{3}$$

However, the ΔH_{LHV} is used very often to express the fuel cell efficiency to compare it with the internal combustion engine, whose efficiency has traditionally been expressed using the fuel ΔH_{LHV}. In this case, the maximum theoretical fuel cell efficiency results in a higher number:

$$\eta_{\text{LHV}} = -\Delta G/ - \Delta H_{\text{LHV}} = 228.74/241.98 = 94.5\%. \tag{4}$$

If both ΔG and ΔH_{LHV} in (3) are divided by $2F$, where 2 is the number of electrons per molecule of H_2 and F is the Faraday number, the fuel cell efficiency may be expressed as a ratio of two potentials:

$$\eta_{\text{HHV}} = \frac{-\Delta G}{-\Delta H_{\text{HHV}}} = \frac{\frac{-\Delta G}{2F}}{\frac{-\Delta H_{\text{HHV}}}{2F}} = \frac{1.23}{1.482} = 83\%, \tag{5}$$

where $\frac{-\Delta G}{2F} = 1.23\text{V}$ is the theoretical cell potential, and $\frac{-\Delta H_{\text{HHV}}}{2F} = 1.482\text{V}$ is the potential corresponding to the ΔH_{LHV}, or thermoneutral potential.

In this section, we analyzed the theoretical fuel cell efficiency. However, as explained in the previous sections, in a real fuel cell the efficiency is quite lower and also depends on the fuel cell current. The fuel cell efficiency η_{FC} can also be defined as the ratio between the power produced and the power of hydrogen consumed [16]:

$$\eta_{\text{HHV}} = \frac{P_{\text{FC}}}{P_{H_2}} = \frac{\frac{V_{\text{fc}} I_{\text{fc}}}{-\Delta H_{\text{HHV}} I_{\text{fc}}}}{2F} = \frac{V_{\text{fc}}}{1.482}, \tag{6}$$

$$\eta_{\text{LHV}} = \frac{P_{\text{FC}}}{P_{H_2}} = \frac{\frac{V_{\text{fc}} I_{\text{fc}}}{-\Delta H_{\text{LHV}} I_{\text{fc}}}}{2F} = \frac{V_{\text{fc}}}{1.254}, \tag{7}$$

where V_{fc} is the generated voltage and I_{fc} is the fuel cell current. Thus, the FC efficiency is related to the actual voltage, which is related to the fuel cell current through the polarization curve.

[4] The Gibbs free energy is used to represent the available energy to do external work. The changes in Gibbs free energy ΔG are negative, which means that the energy is released from the reaction, and varies with both temperature and pressure [18].

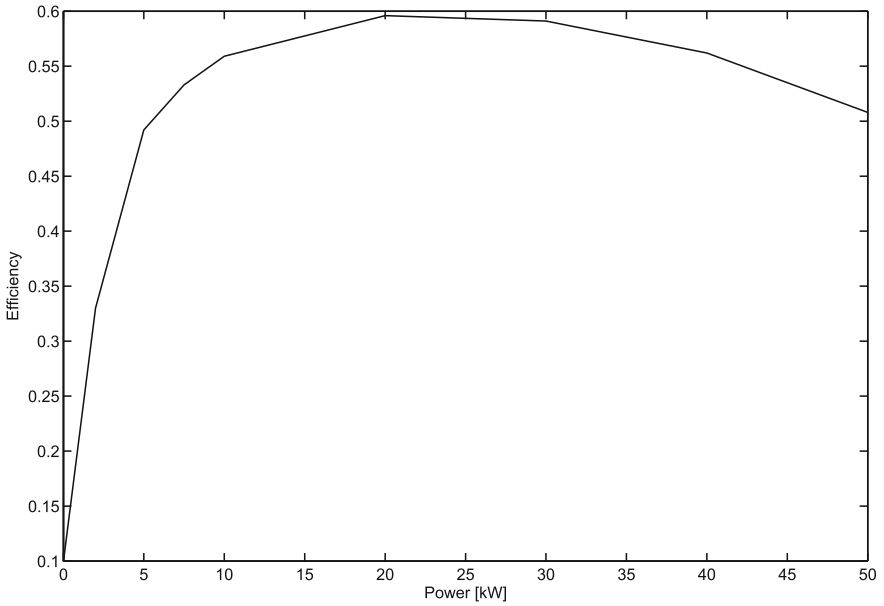

Fig. 3 Efficiency curve of a fuel cell system

Moreover, in a real system it is necessary to incorporate some auxiliary systems which consume a fraction of the generated power. As a result, the efficiency of the fuel cell system, η_{fcs}, is even lower than that expressed in Eq. 6:

$$\eta_{\text{fcs}} = \eta_{\text{HHV}} \frac{P_{\text{net}}}{P_{\text{fc}}} = \eta_{\text{HHV}} \frac{P_{\text{fc}} - P_{\text{aux}}}{P_{\text{fc}}} = \eta_{\text{HHV}} \left(1 - \frac{P_{\text{aux}}}{P_{\text{fc}}}\right), \tag{8}$$

where P_{net} is the net power output, P_{fc} is the fuel cell power, and P_{aux} is the power consumed by the auxiliary components, which include, in particular, the air compressor. The efficiency curve of a fuel cell system of 50 kW modelled in ADvanced VehIcle SimulatOR (ADVISOR)[5] is shown in Fig. 3.

1.5 Generic Structure of a Fuel Cell-Based Power Generation System

In order to be able to produce energy, it is necessary to integrate the fuel cell stack with other components to form a fuel cell-based power generation system. A generic scheme showing the interrelation between the main components of the power generation system is presented in Fig. 4. These components can be divided into the following subsystems [18]:

[5] ADVISOR is a toolbox developed by the national renewable energy laboratory with the aim of analyzing the performance and fuel economy of conventional, electric, and hybrid vehicles [19, 20].

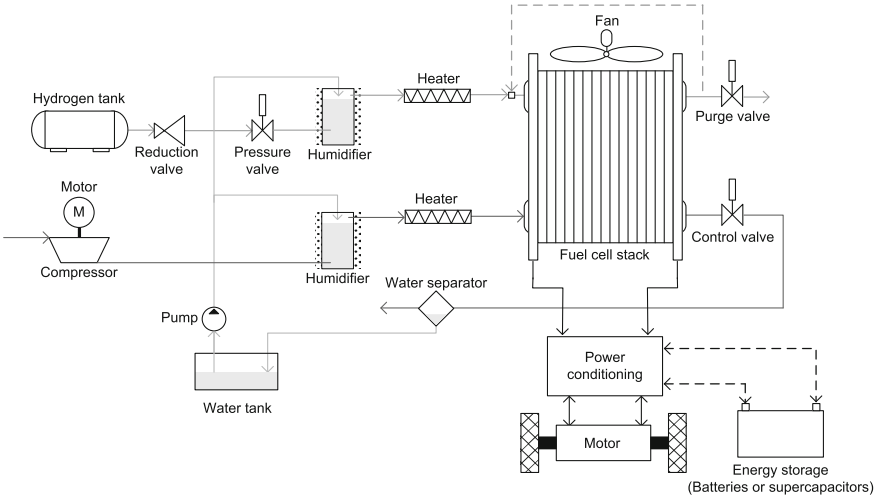

Fig. 4 General scheme of a FCS oriented to automotive applications

1.5.1 Reactant Flow Subsystem

The reactant flow subsystem consists of the hydrogen and air supply circuits. The objective is to supply the adequate reactant flow to ensure fast transient response and minimal auxiliary power consumption. The hydrogen supply circuit is generally composed of a pressurized tank with pure H_2 connected to the anode through a pressure-reduction valve and a pressure-controlled valve, meanwhile, the air supply circuit is generally composed of an air compressor which feeds the cathode with pressurized air from the atmosphere. The anode output is generally operated in *dead-ended* mode and a purge valve in the anode output is periodically opened to remove the water and accumulated nitrogen gas. In case the anode output is not closed it is possible to reinject the out-flowing hydrogen into the anode input. On the other hand, the cathode output is normally open through a fixed restriction. The cathode air supply will be studied in Chap. 3 where we propose to close the cathode output with a controlled valve.

1.5.2 Heat and Temperature Subsystem

The heat and temperature subsystem includes the fuel cell stack cooling system and the reactant heating system. The thermal management of the fuel cell is critical since the performance depends strongly on the temperature. The stack temperature control can be done using a fan or a water refrigeration subsystem.

1.5.3 Water Management Subsystem

The objective of the water management subsystem is to maintain an effective hydration of the polymer membrane and an adequate water balance, because the fuel cell performance is also strongly dependent on membrane hydration. Both the air and the hydrogen, are usually humidified before entering the fuel cell with humidifiers in both circuits. The water that leaves the cathode can be recovered in a water separator and reinjected in the humidifiers through a pump.

1.5.4 Power Conditioning Subsystem

Fuel cells generate an unregulated *DC* voltage which drops off when the current increases according to the polarization curve. In general, some power conditioning actions are necessary to supply the load properly. Such actions make necessary the use of *DC/DC* regulators and/or inverter regulators.

1.5.5 Power Management Subsystem

The power management subsystem controls the power drawn from the fuel cell stack. If no energy storage devices are used, the full load must be supplied by the fuel cell and no power management is necessary. However, if an energy storage system is included, such as batteries or supercapacitors, it is necessary to implement a power management between these two power sources. A review of fuel cell hybrid systems is described in the following section and a detailed study is done in Chap. 4.

1.6 Modeling of Polymer Electrolyte Membrane Fuel Cell Systems

Validated mathematical models provide powerful tools for the development and improvement of fuel cell-based systems. Mathematical models can be used to describe the fundamental phenomena that take place in the system to predict the behavior under different operating conditions and to design and optimize the control of the system.

The fuel cell system models describe quantitatively the physical and electrochemical phenomena that take place in to the cells. The models can be divided into two groups [3]: empirical models and mechanistic models. Most of the empirical models are focused on the prediction of the polarization curve, which is used to characterize the electrical operation of the FC, by means of empirical equations. The following empirical equation developed by Kim et al. [21] is used to calculate the voltage (E) at different current densities (J), fitting experimental data at several temperatures, pressures, and oxygen compositions in the cathode gas mixture:

$$E = E_0 - b\log J - RJ - m\exp(nJ), \tag{9}$$

where E_0 is the thermodynamic open-circuit voltage. The exponential term characterizes the mass-transport region of the polarization curve, the zone where the increase in slope of the pseudo-linear region and the subsequent rapid fall-off of the cell potential. The parameter n has more pronounced effects than the parameter m in this region. The terms E_0 and b yield the electrode kinetic parameters for oxygen reduction in the cell. R represents the resistance, predominantly ohmic, and, slightly, the charge-transfer resistance of the electro-oxidation of hydrogen.

Later, Squadrito et al. [22] used an empirical approach to account the mass transport limitation, modifying the model of Kim et al. by replacing the last term of (9) with $\left[mJ^n \ln\left(1 - J/J_{\text{lim}}\right)\right]$ where m and n are empirically determined constants and J_{lim} is the limiting current density obtained by fitting experimental data. The equation describes experimental data over the full range of current density taking into account possible mass transport limitations. The empirical equation was used to fit experimental data obtained from a single cell, showing good agreement between theoretical and experimental data.

One example of an empirical model widely used is the model developed by Amphlett et al. [14], which incorporates as much empirical properties as mechanistic to obtain a transient model able to predict the FC voltage as a function of the current, the FC temperature and the hydrogen and oxygen partial pressures for a 35-cell 5 kW PEM fuel cell. The model works well for the experimental system in study but can be generalized to any other system recalculating the values of the model.

On the other hand, the mechanistic model considers the fundamental phenomena in detail such as, heat and mass transport, forces, and electrochemical processes. Mechanistic modeling (single and multi-domain) has been utilized to study a wide range of phenomena including polarization effects (activation, ohmic and concentration overpotentials), water management, thermal management, CO kinetics, catalyst utilization and flow field geometry [23]. All these models are parametric in the sense that they account for the cell performance of various input parameters, typically temperature, pressure and humidity.

Many of the mechanistic models are one-dimensional where only the direction across the fuel cell is taken into account. Some of the first works dealing with this type of models are [24–26]. Then two-dimensional and three-dimensional models were developed. Some two-dimensional models describe the plane perpendicular through the flow channels [27, 28] while others simulate the fuel cell along the flow channels [29, 30]. Within the three-dimensional models can be mentioned the model developed by Nguyen et al. [31], which is a three-dimensional model of a PEM fuel cell with serpentine gas channels, and the model developed by Natarajan [32].

Some of the earlier works focused in the humidification problem, addressing the humidification requirements of the inlet gases to maintain the water balance [33]. Fuller and Newman [34] also addressed the water and thermal management, similar to Nguyen and White [29] who studied different forms of gas humidification and water management, analyzing the cell performance. The model of Wöhr et al. [35] showed that for fuel cell stacks water management becomes even more difficult and

is strongly related to thermal management. The temperatures of the inner cells of the stack are higher than the outer cells resulting in membrane dehydration.

Another approach to fuel cell modeling is the use of equivalent circuits to represent the system behavior. In fact, one of the most attractive aspects of the Electrochemical Impedance Spectroscopy as a tool for investigating the electrical and electrochemical properties of materials and systems, is the direct connection that often exists between the behavior of a real system and that of an idealized model circuit consisting of discrete electrical components [36]. The procedure typically consist in the comparison or fitting the impedance data to an equivalent circuit, which is representative of the physical processes taking place in the system under investigation. There are analogies between the circuit elements and the electrochemical processes, so that the results of data fitting can be more easily converted into physical understanding.

Many authors have studied the modeling approach based on equivalent electrical circuits, consisting of an arrangement of different electrical components to have the same frequency response as that obtained by electrochemical impedance spectroscopy tests [37–40]. Some works present equivalent circuits using electrical elements, such as resistances, capacitances or inductance. However, other works use additional distributed elements that represent electrochemical or mass and ionic transport phenomena. For example, Warburg impedance represents the impedance of one-dimensional distributed diffusion of a species in an electrode. Another example is a constant phase element, used for describing a distributed charge accumulation on rough irregular electrode surfaces.

However, there are some problems in using analogies to describe electrochemical systems: one of them is that different equivalent circuits obtain the same frequency response, another problem is the overlapping frequency response of different phenomena and the dependence of the electrochemical phenomena on the operating conditions (temperature, current, pressure, etc.).

So far we have seen different types of models that study the cell behavior in both stationary and transient states. Nevertheless, there are few dynamic models suitable for control purposes. In the work of Pukrushpan et al. [4] a dynamic model for PEMFCS that is suitable for the control study has been developed. The model captures the transitory behavior of the air compressor, the gases filling dynamics (in the cathode and anode), and the effect of the membrane humidity. These variables affect the cell voltage and, therefore, the efficiency and the output power. The polarization curve in this model is a function of the hydrogen and oxygen partial pressures, the stack temperature and the membrane water content. This allows to evaluate the effect of variations of oxygen concentration and membrane humidity in the output voltage, which are necessary to make the control during transitory operation.

Another practical model oriented to control was developed by Del Real et al. [41] where the model parameters have been adjusted specifically for a 1.2 kW Ballard stack, which is considered a benchmark as it is widely used by research groups in the PEM fuel cell field. The model can predict both steady and transient states subject to variable loads (including flooding and anode purges), as well as the system start-up. The proposed model methodology is accurate since the simulated results show good agreement, compared to experimental data from the Ballard stack.

On the other hand, a dynamic model which incorporates the effects of charge double layer capacitance, the dynamics of flow and pressure in the anode and cathode channels and mass/heat transfer transient features in the fuel cell body has been presented [42]. This dynamic model can predict the transient response of cell voltage, temperature of the cell, hydrogen/oxygen out-flow rates and cathode and anode channel temperatures/pressures under sudden change in load current. The simulation results are analyzed and compared to benchmark results, reporting that a good agreement is found between tests and simulations. Similarly, a dynamic electrochemical model of a grid independent fuel cell power plant is presented in [43]. The model includes the methanol reformer, the PEM stack and the power conditioning unit. The model is used to predict the output voltage when subjected to rapid changes in a residential load connected to it, showing a high degree of accordance. More recently, a semi-empirical dynamic model for stack voltage, based on experimental investigation, was presented [44]. The proposed model can predict the transient response of stack voltage under step change in current with good agreement between tests and simulations.

The model developed by Pukrushpan et al. [4], which has been employed in several works for control purposes [45–51], is utilized in this book as a base to represent the behavior of a generic fuel cell system. The model is described in detail in Sects. 1 and 2.

1.7 Description of the Fuel Cell System Model

The model developed by Pukrushpan et al. [4] is used in several chapters of this book as a base to characterize the dynamic behavior and performance of PEM fuel cell systems. This model contains four main subsystems that interact with each other:

- FC voltage subsystem
- Membrane hydration subsystem
- Cathode flow subsystem
- Anode flow subsystem

The spatial variation of the parameters is not considered and, thus, they are treated as lumped parameters. On the other hand, the time constants of the electrochemical reactions are in the order of magnitude of 10^{-19} s despite another work [52] argues that this constants are significatively lower (10^{-9} s). In any case, all the literature agrees in the fastness of the electrochemical reactions, as remarked in [53] and [42]. Thus, for control purpose, these time constants can be assumed negligible compared to other constants much slower: temperature (10^{2} s) and dynamics of volume filling (10^{-1} s).

In this book, this base model has been modified to adapt it to the proposed control structures described in Sect. 2. In the original model there is only one control variable: the compressor motor voltage. In this book, it is proposed to add an extra variable, the throttle opening area in the cathode output (A_t), adding a control valve in the

cathode output. The advantages of this new configuration are covered in detail in Sect. 2.3.

Usually, in model-based control, it is necessary to find simplified models, derived from the complete ones or from experimental data, to be used as inner models into the controller. Here, the step response is utilized to obtain a simplified model that is used as internal model to predict the future process response in the control strategy implemented in Sect. 2. The main advantage of this simplified model is that it is easily obtainable through experimental data with good agreement with respect to the original nonlinear system in the considered operating point.

1.8 Principal Equations in the Fuel Cell System Model

The model described in the previous section has the following governing equations where the mass of air in the supply manifold, the masses of oxygen, nitrogen and water in the cathode and the masses of hydrogen and water in the anode are defined using the principle of mass conservation [45]:

$$\frac{\mathrm{d}m_{\mathrm{sm}}}{\mathrm{d}t} = W_{\mathrm{cp}} - W_{\mathrm{sm,out}}, \tag{10}$$

$$\frac{\mathrm{d}m_{\mathrm{O_2,ca}}}{\mathrm{d}t} = W_{\mathrm{O_2,ca,in}} - W_{\mathrm{O_2,ca,out}} - W_{\mathrm{O_2,rct}}, \tag{11}$$

$$\frac{\mathrm{d}m_{\mathrm{N_2,ca}}}{\mathrm{d}t} = W_{\mathrm{N_2,ca,in}} - W_{\mathrm{N_2,ca,out}}, \tag{12}$$

$$\frac{\mathrm{d}m_{w,\mathrm{ca}}}{\mathrm{d}t} = W_{v,\mathrm{ca,in}} - W_{v,\mathrm{ca,out}} - W_{v,\mathrm{ca,gen}} + W_{v,m}, \tag{13}$$

$$\frac{\mathrm{d}m_{\mathrm{H_2}}}{\mathrm{d}t} = W_{\mathrm{H_2,an,in}} - W_{\mathrm{H_2,an,out}} - W_{\mathrm{H_2,rct}}, \tag{14}$$

$$\frac{\mathrm{d}m_{w,\mathrm{an}}}{\mathrm{d}t} = W_{v,\mathrm{an,in}} - W_{v,\mathrm{an,out}} - W_{v,m} - W_{l,\mathrm{an,out}}, \tag{15}$$

where

- W_{cp} is the compressor flow,
- $W_{\mathrm{sm,out}}$ is the outlet mass flow,
- $W_{\mathrm{O_2,ca,in}}$ is the mass flow rate of oxygen gas entering the cathode,
- $W_{\mathrm{O_2,ca,out}}$ is the mass flow rate of oxygen leaving the cathode,
- $W_{\mathrm{O_2,rct}}$ is the mass flow rate of oxygen reacted,
- $W_{\mathrm{N_2,ca,in}}$ is the mass flow rate of nitrogen gas entering the cathode,
- $W_{\mathrm{N_2,ca,out}}$ is the mass flow rate of nitrogen gas leaving the cathode,
- $W_{v,\mathrm{ca,in}}$ is the mass flow rate of vapor entering the cathode,
- $W_{v,\mathrm{ca,out}}$ is the mass flow rate of vapor leaving the cathode,
- $W_{v,\mathrm{ca,gen}}$ is the rate of vapor generated in the fuel cell reaction,

- $W_{v,\text{menbr}}$ is the mass flow rate of water across the fuel cell membrane,
- $W_{l,\text{ca,out}}$ is the mass flow rate of liquid water leaving the cathode,
- $W_{\text{H}_2,\text{an,in}}$ is the mass flow rate of hydrogen gas entering the anode,
- $W_{\text{H}_2,\text{an,out}}$ is the mass flow rate of hydrogen gas leaving the anode,
- $W_{\text{H}_2,\text{rct}}$ is the rate of hydrogen reacted,
- $W_{v,\text{an,in}}$ is the mass flow rate of vapor entering the anode,
- $W_{v,\text{an,out}}$ is the mass flow rate of vapor leaving the anode,
- $W_{v,m}$ is the mass flow rate of water transfer across the fuel cell membrane, and
- $W_{l,\text{an,out}}$ is the rate of liquid water leaving the anode.

The voltage of a fuel cell stack consisting of n fuel cells is given as

$$v_{\text{st}} = n \cdot v_{\text{fc}}, \tag{16}$$

where the voltage of a single fuel cell is defined as

$$v_{\text{fc}} = E - v_{\text{act}} - v_{\text{ohm}} - v_{\text{conc}} \tag{17}$$

with E being the open circuit voltage and v_{act}, v_{ohm} and v_{conc} being the activation, ohmic and concentration overpotentials, respectively. By fitting experimental data to the phenomenological model equations, the open circuit voltage and the three overpotentials are respectively defined as

$$\begin{aligned} E = {} & 1.229 - 0.85 \times 10^{-3}(T_{\text{fc}} - T_{\text{amb}}) \\ & + 4.3085 \times 10^{-5} T_{\text{fc}} \times \left[\ln(1.01325 p_{\text{H}_2}) + \frac{1}{2} \ln(1.01325 p_{\text{O}_2}) \right]. \end{aligned} \tag{18}$$

The activation voltage is

$$v_{\text{act}} = v_0 + v_a(1 - e^{c_1 i}) \tag{19}$$

with

$$\begin{aligned} v_0 = {} & 0.279 - 8.5 \times 10^{-4}(T_{\text{fc}} - T_{\text{amb}}) + 4.308 \times 10^{-5} T_{\text{fc}} \\ & \times \left[\ln\left(\frac{p_{\text{Ca}} - p_{\text{sat}}(T_{\text{fc}})}{1.01325} \right) + \frac{1}{2} \ln\left(\frac{0.1173(p_{\text{Ca}} - p_{\text{sat}}(T_{\text{fc}}))}{1.01325} \right) \right], \end{aligned} \tag{20}$$

$$\begin{aligned} v_a = {} & (-1.618 \times 10^{-5} T_{\text{fc}} + 1.618 \times 10^{-2}) \\ & \times \left(\frac{p_{\text{O}_2}}{0.1173} + p_{\text{sat}}(T_{\text{fc}}) \right]^2 \\ & + (1.8 \times 10^{-4} T_{\text{fc}} - 0.166) \left(\frac{p_{O_2}}{0.1173} + p_{\text{sat}}(T_{\text{fc}}) \right) \\ & (-5.8 \times 10^{-4} T_{\text{fc}} + 0.5736), \end{aligned} \tag{21}$$

and

$$c_1 = 10. \tag{22}$$

The ohmic voltage is

$$v_{\text{ohm}} = i\,R_{\text{ohm}} \tag{23}$$

with the fuel cell electrical resistance

$$R_{\text{ohm}} = \frac{t_m}{\sigma_m}, \tag{24}$$

the membrane conductivity

$$\begin{aligned} &\sigma_m = (b_{11}\mu_m - b_{12}) \exp\left[b_2\left(\frac{1}{303} - \frac{1}{T_{\text{fc}}}\right)\right] \\ &b_{11} = 5.139 \times 10^{-3}, \qquad b_{12} = 3.26 \times 10^{-3}, \qquad b_{12} = 350 \end{aligned} \tag{25}$$

and

$$v_{\text{conc}} = i\left(c_2 \frac{i}{i_{\max}}\right)^{c_3} \tag{26}$$

with

$$c_2 = \begin{cases} (7.16 \times 10^{-4} T_{\text{fc}} - 0.622)\left(\frac{p_{O_2}}{0.1173} + p_{\text{sat}}(T_{\text{fc}})\right) \\ \quad +(-1.45 \times 10^{-3} T_{\text{fc}} + 1.68) \quad \text{for } \left(\frac{p_{O_2}}{0.1173} + p_{\text{sat}}(T_{\text{fc}})\right) < 2\,\text{atm} \\ (8.66 \times 10^{-5} T_{\text{fc}} - 0.068)\left(\frac{p_{O_2}}{0.1173} + p_{\text{sat}}(T_{\text{fc}})\right) \\ \quad +(-1.6 \times 10^{-4} T_{\text{fc}} + 0.54) \quad \text{for } \left(\frac{p_{O_2}}{0.1173} + p_{\text{sat}}(T_{\text{fc}})\right) \geq 2\,\text{atm} \end{cases} \tag{27}$$

and

$$i_{\max} = 2.2, \quad c_3 = 2. \tag{28}$$

The governing equations for the supply manifold pressure and the return manifold pressure are respectively defined using the energy conservation principle and the standard thermodynamics relationships as follows:

$$\frac{\mathrm{d}p_{\text{sm}}}{\mathrm{d}t} = \frac{\gamma R_a}{V_{\text{sm}}}(W_{\text{cp}} T_{\text{cp}} - W_{\text{sm,out}} T_{\text{sm}}), \tag{29}$$

$$\frac{\mathrm{d}p_{\text{rm}}}{\mathrm{d}t} = \frac{R_a T_{\text{rm}}}{V_{\text{rm}}}(W_{\text{ca,out}} - W_{\text{rm,out}}), \tag{30}$$

where V_{sm} is the supply manifold volume, V_{rm} is the return manifold volume, T_{sm} is the supply manifold air temperature, T_{rm} is the return manifold air temperature,

T_{cp} is the temperature of the air leaving the compressor, R_a is the air gas constant, and γ is the air specific heat ratio.

To express the governing equations in terms of the states, the closure relations Eqs. 31–38 are used. The supply manifold outlet air rate $W_{sm,out}$ is related to the supply manifold pressure p_{sm} and the cathode pressure p_{ca} via the linearized nozzle equation:

$$W_{sm,out} = k_{sm,out}(p_{sm} - p_{ca}), \tag{31}$$

where $k_{sm,out}$ is the supply manifold outlet orifice constant.

The inlet oxygen, nitrogen, and cathode vapour mass flow rates, $W_{O_2,in}$, $W_{N_2,in}$, and $W_{v,ca,in}$ are related to the cathode inlet air mass flowrate, the inlet air humidity and the mass fraction of oxygen and nitrogen in dry air using the ideal gas relations. The outlet oxygen, nitrogen and cathode vapour mass flow rates, $W_{O_2,out}$, $W_{N_2,out}$, and $W_{v,ca,out}$, are likewise related to the outlet air mass flowrate, the outlet air humidity and the mass fraction of the oxygen and nitrogen in dry air at the cathode outlet using the ideal gas relations. The reacted oxygen and hydrogen and generated water vapor (in the cathode) mass flow rates, $W_{O_2,rct}$, $W_{H_2,rct}$, and $W_{v,ca,gen}$, are related to the fuel cell current:

$$W_{O_2,rct} = M_{O_2}\frac{nI_{fc}}{4F}, \tag{32}$$

$$W_{H_2,rct} = M_{H_2}\frac{nI_{fc}}{2F}, \tag{33}$$

$$W_{v,ca,gen} = M_v\frac{nI_{fc}}{2F}, \tag{34}$$

where the constants 4 and 2 in the denominators denote the of electrons involved in the oxidation and the reduction half-reactions respectively, M_{O_2} is the molar mass of oxygen, M_{H_2} is the molar mass of hydrogen, M_v is the molar mass of vapor, and F is the Faraday constant.

The water mass flowrate through the membrane, $W_{v,m}$, is defined using the hydration model. The outlet hydrogen and water masses are assumed to be zero, that is, hydrogen is assumed to react completely in the anode, while water generated by the oxidation half-reaction is assumed to be transported via electro-osmosis through the membrane towards the cathode.

The governing equation for the rotational speed of the compressor is defined by the power conservation principle as

$$J_{cp}\frac{d\omega_{cp}}{dt} = \tau_{cm} - \tau_{cp}, \tag{35}$$

where J_{cp} is the combined inertia of the compressor and the motor ($kg.m^2$), ω_{cp} is the compressor speed (rad/sec), τ_{cm} is the compressor motor torque input (Nm)

calculated in Eq. 36, and τ_{cp} is the torque required to drive the compressor (Nm) calculated in Eq. 37.

The compressor motor torque τ_{cm} is related to the compressor motor voltage V_{cm} and the compressor motor rotational speed ω_{cp} by the static motor equation:

$$\tau_{cm} = \eta_{cm} \frac{k_t}{R_{cm}} \left(V_{cm} - k_v . \omega_{cp} \right), \tag{36}$$

where k_t, R_{cm}, and k_v are motor constants and η_{cm} is the motor mechanical efficiency. The steady state compressor torque τ_{cp} is related to the supply manifold pressure, the compressor motor rotational speed and the compressor air flowrate W_{cp} via the thermodynamic relations

$$\tau_{cp} = \frac{C_P}{\omega_{cp}} \frac{T_{atm}}{\eta_{cp}} \left[\left(\frac{p_{sm}}{p_{atm}} \right)^{(\gamma-1)/\gamma} - 1 \right] W_{cp}, \tag{37}$$

where C_p is the air specific heat, η_{cp} is the compressor efficiency, and T_{atm} and p_{atm} are the atmospheric temperature and pressure, respectively.

The air temperature in the compressor, T_{cp}, is defined using basic thermodynamic relations

$$T_{cp} = T_{atm} + \frac{T_{atm}}{\eta_{cp}} \left[\left(\frac{p_{sm}}{p_{atm}} \right)^{(\gamma-1)/\gamma} - 1 \right]. \tag{38}$$

The air temperature in the supply manifold, T_{sm}, is obtained from m_{sm}, p_{sm} and V_{sm} using the ideal gas law. The cathode outlet air flowrate $W_{ca,out}$ is related to the cathode pressure and return manifold pressure via a linearized nozzle equation analogous to Eq. 31. The return manifold outlet air flowrate $W_{rm,out}$ is defined using a non-linearized nozzle relation as discussed in Sect. 2.2, while the return manifold air temperature T_{rm} is considered to be constant and equal to the temperature of the fuel cell stack.

The flowrate of water through the membrane is controlled by two transport phenomena: electroosmotic drag of water molecules by the protons and back-diffusion from the cathode towards the anode. The transport phenomena is defined as

$$W_{v,m} = M_v A_{fc} n \left(n_d \frac{i}{F} - D_w \frac{(C_{v,ca} - C_{v,an})}{t_m} \right), \tag{39}$$

where the electroosmotic drag coefficient is given as

$$n_d = 0.0029 \mu_m^2 + 0.05 \mu_m - 3.4 \times 10^{-19} \tag{40}$$

and μ_m is the mean water content in the membrane. The water content is defined as

$$u_i = \begin{cases} 0.043 + 17.81 a_i - 39.85 a_i^2 + 36.0 a_i^3, & 0 < a_i \leq 1 \\ 14 + 1.4(a_i - 1), & 1 < a_i \leq 3 \\ & (i = m, \text{an}, \text{ca}) \end{cases} \tag{41}$$

where the water vapour activity is defined as

$$a_i = \frac{x_{v,i}\, p_i}{p_{\text{sat,i}}} = \frac{p_{v,i}}{p_{\text{sat,i}}} \quad (i = \text{an, ca}). \tag{42}$$

The average water vapour activity in the membrane is defined as

$$a_m = \frac{a_{\text{an}} + a_{\text{ca}}}{2} \tag{43}$$

and the water diffusion coefficient is given as

$$D_W = D_\lambda \exp\left[2416\left(\frac{1}{303} - \frac{1}{T_{\text{fc}}}\right)\right] \times 10^{-4} \tag{44}$$

with the preexponential term

$$D_\lambda = \begin{cases} 10^{-6}, & \mu_m < 2 \\ 10^{-6}[1 + 2(\mu_m - 2)], & 2 \le \mu_m \le 3 \\ 10^{-6}[3 - 1.67(\mu_m - 3)], & 3 < \mu_m < 4.5 \\ 1.25 \times 10^{-6}, & \mu_m \ge 4.5 \end{cases} \tag{45}$$

The water concentration at the membrane surfaces on anode and cathode sides in Eq. 39 is a function of the membrane water content

$$C_{v,i} = \frac{\rho_{m,\text{dry}}}{M_{m,\text{dry}}}\mu_i \quad (i = \text{an, ca}), \tag{46}$$

where $\rho_{m,\text{dry}}$ (kg/cm^3) is the membrane dry density and $M_{m,\text{dry}}$ (kg/mol) is the equivalent weight.

2 Auxiliary Equipment and System Modeling

While the fuel cell operates with oxygen as reactant in the cathode, it is more practical to use oxygen from air. Air is mainly composed of nitrogen (78.084%), oxygen (20.946%), and argon (0.9340%). The effect of using air instead of pure oxygen is a reduction of approximately 50 mV in the cell voltage [16]. Additionally, there is a reduction in the fuel cell efficiency because of the power consumption to pump the oxygen and almost four times that of nitrogen.

In a hydrogen-air fuel cell system the air is supplied by a fan, a blower or a compressor. In any case, there is an electric motor with a power consumption that implies a reduction in the efficiency of the fuel cell system. The net power output, P_{net}, that is actually available is the fuel cell power, P_{fc}, less the power consumed by the ancillary components, P_{aux}, which includes the compressor or the blower:

$$P_{\text{net}} = P_{\text{fc}} - P_{\text{aux}}. \tag{47}$$

The principal consumption between the ancillary equipments is that corresponding to the electric motor that runs the compressor or the blower. Besides, it depends strongly on the operating conditions. Thus, it can be assumed that the consumption of the ancillary equipments is the consumption of this electric motor.

When the fuel cell operates at high pressures, the power output is higher. Thus, the most common scenario is a fuel cell where the cathode is supplied with air by a compressor. However, the power consumption of the compressor increases significantly with the pressure. Thus, when the compressor consumption is taken into account, there is a trade-off between pressure and efficiency.

The operation of the fuel cell system at high pressures increases the generated voltage as a result of the increase in the cathode oxygen partial pressure and anode hydrogen partial pressure (see Eq. 1). Especially, an increase in the cathode pressure produces an increase in the supply manifold pressure and thus, an increase in the pressure ratio across the compressor and in the compressor power consumption contributing to a reduction in the system efficiency. The power consumed by the air compressor is

$$P_{\text{cp}} = \frac{C_p T_{\text{atm}}}{\eta_{\text{cp}}} \left[\left(\frac{p_{\text{sm}}}{p_{\text{atm}}}^{\frac{\gamma-1}{\gamma}} \right) - 1 \right] W_{\text{cp}}, \tag{48}$$

where W_{cp} is the compressor air flow rate, P_{cp} is the compressor power, T_{atm} is the inlet air temperature in the compressor, η_{cp} is the compressor efficiency, p_{sm} is the supply manifold pressure, $C_p = 1{,}004\,\text{J}\,\text{kg}^{-1}\,\text{K}^{-1}$ is the specific heat capacity of air, and $\gamma = 1.4$ is the ratio of the specific heat of air. Actually, the power consumed by the electric motor is higher because of the mechanical and electric inefficiencies:

$$P_{\text{EM}} = \frac{P_{\text{comp}}}{\eta_{\text{mec}} \cdot \eta_{\text{EM}}}, \tag{49}$$

where η_{mec} is the compressor mechanical efficiency and η_{EM} is the efficiency of the electric motor. In Chap. 3 will be seen how this power consumption affects the efficiency of the system. Besides, a solution from the point of view of control will be studied in detail.

3 Optimal Operation of the FCS

The FCS model is useful to study the optimal operation of an FCS, especially at low loads. An adequate operation produces important benefits, increasing the system efficiency in terms of hydrogen reduction and allowing a greater peak power. In a direct-hydrogen FCS with the cathode supplied with air through a compressor, the air supply subsystem has a crucial role in the improvement of the performance

of the system [10]. In fact, there are two external variables that have greater impact on the polarization curve: the air pressure and the air stoichiometry.

The air pressure and the air stoichiometry control the oxygen partial pressure in the catalytic layer of the cathode, which determines the cathode polarization and, therefore, the efficiency. In [54], it is also stated the importance of the air pressure control to improve the FCS efficiency. The efficiency improvement for a given load is based on a trade-off between the increase of the air pressure and the air stoichiometry, and the increase of the parasitic compressor power.

In the work of Friedman and Moore [55], it is shown that an FCS can be optimized to obtain high peak power and high efficiency over a broad range of output powers. The key to obtain this objective is to vary the pressure and the air flow. Based on this result, it can be concluded that an FCS must be operated to the greater possible pressure and air stoichiometry. Nevertheless, if the energy necessary to compress the air is considered, the result is different: for a fixed air flow, the compressor power consumption increases significantly when the pressure is increased. This means that it is possible to find an optimal combination of pressure and air flow.

A similar conclusion is stated in [45]. In this work, it is assumed that the FCS net power P_{net} can be approximately defined as the difference between the power produced by the FCS, P_{fcs}, and the consumed compressor power P_{cm}. For each load current I_{st}, an air flow increment increases the cathode pressure and, therefore, increases the oxygen partial pressure, increasing the FCS voltage. This also leads to an increment in the oxygen excess ratio in the cathode, λ_{O_2}. The initial increase in the oxygen excess is translated into an FCS power increase and a net FCS power. Nevertheless, if a limit λ_{O_2} is exceeded, an excessive compressor power is produced so that the net power falls.

Following this analysis and using the model, it is possible to find the optimal relation among maximum net power, $P_{\text{max}}^{\text{net}}$, optimal oxygen ratio, $\lambda_{O_2}^{\text{opt}}$, optimal supply manifold air pressure, $p_{\text{SM}}^{\text{opt}}$, and optimal compressor motor voltage, $v_{\text{CM}}^{\text{opt}}$, with the stack current, I_{st} [45]. These relations are shown in Eqs. 50–53 and also in Fig. 5.

$$P_{\text{max}}^{\text{net}} = -2.99 \times 10^{-4} I_{\text{st}}^2 + 0.271 I_{\text{st}} - 0.871 \tag{50}$$

$$\lambda_{O_2}^{\text{opt}} = -2.7633 \times 10^{-6} I_{\text{st}}^2 - 15.931 \times 10^{-4} I_{\text{st}} + 2.7331 \tag{51}$$

$$p_{\text{SM}}^{\text{opt}} = 2.9996 I_{\text{st}}^2 + 736.4 I_{\text{st}} + 8.932 \times 10^4 \tag{52}$$

$$v_{\text{CM}}^{\text{opt}} = -1.36 \times 10^{-3} I_{\text{st}}^2 + 1.17 I_{\text{st}} + 14.3 \tag{53}$$

The Eq. 51 expresses that at each level of the stack current there is an optimal value of λ_{O_2} at which P_{net} has the maximum value. This optimal value in the oxygen excess ratio is achieved by applying a compressor voltage according to Eq. 53. The Eqs. 50–53 are obtained by solving the model equations previously shown under steady-state condition and the analysis corresponds to the typical fuel cell operating conditions (fuel cell temperature $T_{\text{fc}} = 353\,\text{K}$ and relative humidity $\phi_{\text{Ca}} = 1$).

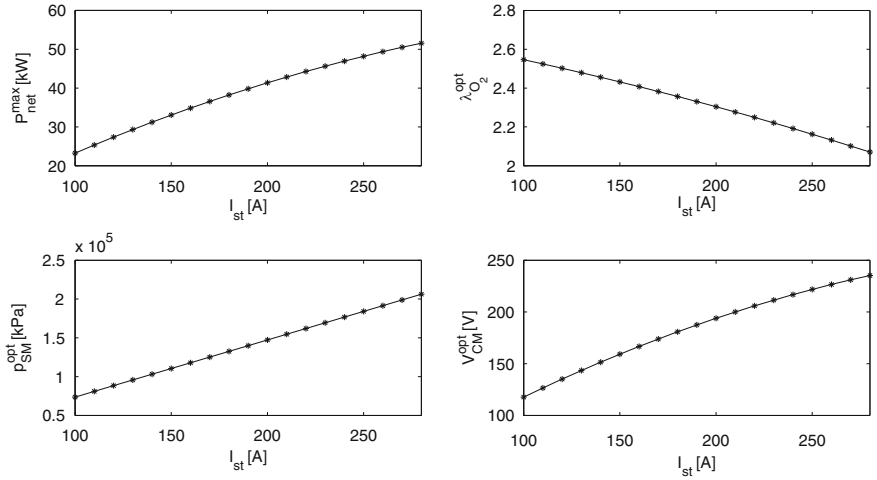

Fig. 5 Optimal relations of $P_{\max}^{\text{net}}$, $\lambda_{O_2}^{\text{opt}}$, $P_{\text{SM}}^{\text{opt}}$, and $v_{\text{CM}}^{\text{opt}}$ as a function of the stack current I_{st}

4 Conclusions

This chapter presents the main concepts about PEM fuel cell systems, showing the structure of these systems, the advantages and disadvantages, and, particularly, the expressions corresponding to the fuel cell voltage and efficiency. Also, different approaches for modeling are presented. Accordingly, a review of PEM fuel cell model has been done. Fuel cell models may be classified into one of three categories: analytic, semi-empirical or mechanistic (theoretical). Among these models, a model widely used in the literature for control purposes is described in detail. Using this model, the influence of the auxiliary equipment in the system efficiency is analyzed and the model is also used to study the optimal operation of a PEM fuel cell system, finding an optimal compressor voltage for each current load that maximizes the net output power. Similarly, this dynamic model is used as a base model in the other chapters of this book.

References

1. Laughton MA (2002) Fuel cells. Power Eng J 16:37–47
2. Tang H, Peikang S, Jiang SP, Wang F, Pan M (2007) A degradation study of Nafion proton exchange membrane of PEM fuel cells. J Power Sources 170(1):85–92
3. Yao K, Karan K, McAuley K, Oosthuizen P, Peppley B, Xie T (2004) A review of mathematical models for hydrogen and direct methanol polymer electrolyte membrane fuel cells. Fuel Cells 4(1–2):3–29
4. Pukrushpan JT, Peng AGH (2002) Modeling and control for PEM fuel cell stack system. American Control Conference, Proceedings of the 2002, 4:3117–3122

5. D'Arco S, Ianuzzi D, Pagano M, Tricoli P (2005) Design criteria optimizing the use of fuel cell source in electric power system. In: Proceedings of the 16th IFAC World Congress, Prague
6. Zhang J, Xie Z, Zhang J, Tang Y, Song C, Navessin T, Shi Z, Song D, Wang H, Wilkinson DP, Liu Z-S, Holdcroft S (2006) High temperature pem fuel cells. J Power Sources 160(2):872–891
7. Carrette L, Friedrich K, Stimming U (2001) Fuel cells-fundamentals and applications. Fuel Cells 1(1):5–39
8. Rajashekara K (2000) Propulsion system strategies for fuel cell vehicles. Fuel Cell Technol for Vehicles 1:179–187
9. Jeong K, Oh B (2002) Fuel economic and life-cycle cost analysis of a fuel cell hybrid vehicle. J Power Sources 105:58–65
10. Friedman D, Moore R (1998) PEM fuel cell system optimization. In: Proc Electrochem Soc 27:407–423
11. EG & G Technical Services, Inc. Science Applications International Corporation (2002) IN: U.S. Department of Energy, Fuel Cell Handbook, 6th edition, Morgantown, West Virginia, USA
12. Flipsen S (2006) Power sources compared: the ultimate truth? J Power Sources 162:927–934
13. Larminie J, Dicks A (2003) Fuel Cell Systems Explained, 2nd edn Wiley, New York, USA
14. Amphlett J, Mann R, Peppley B, Roberge P, Rodrigues A (1996) A model predicting transient responses of proton exchange membrane fuel cells. J Power Sources 61:183–188
15. Correa J, Farret F, Canha L, Simoes M (2004) An electrochemical-based fuel-cell model suitable for electrical engineering automation approach. Ind Electron, IEEE Trans on 51(5):1103–1112
16. Barbir F (2005) PEM fuel cells: theory and practice. Elsevier, Burlington, MA, USA
17. Bossel U (2003) Well-to-wheel studies, heating values, and the energy conservation principle. IN:Ulf Bossel (ed) European Fuel Cell Forum, October 2003, Oberrohrdorf, Switzerland 1:1–5
18. Pukrushpan J (2003) Modelling and control of fuel cell systems and fuel processors. PhD thesis, University of Michigan, Ann Arbor, Michigan, USA. http://www-personal.umich.edu/~annastef/FuelCellPdf/pukrushpan_thesis.pdf
19. Wipke K, Cuddy M, Burch S (1999) Advisor 2.1: a user-friendly advanced powertrain simulation using a combined backward/forward approach. IEEE Trans on Vehicular Technol 48:1751–1761
20. Markel T, Brooker A, Hendricks T, Johnson V, Kelly K, Kramer B, O'Keefe M, Sprik S, Wipke K (2002) Advisor: a system analysis tool for advanced vehicle modeling. J Power Sources 110:255–266
21. Kim J, Lee SM, Srinivasan S, Chamberlin CE (1995) Modeling of proton exchange membrane fuel cell performance with an empirical equation. J Electrochem Soc 142:2670
22. Squadrito G, Maggio G, Passalacqua E, Lufrano F, Patti A (1999) An empirical equation for polymer electrolyte fuel cell (PEFC) behaviour. J Appl Electrochem 29(12):1449–1455
23. Cheddie D, Munroe N (2005) Review and comparison of approaches to proton exchange membrane fuel cell modeling. J Power Sources 147(1–2):72–84
24. Bernardi DM, Verbrugge MW (1991) Mathematical model of a gas diffusion electrode bonded to a polymer electrolyte. AIChE J 37(8):1151–1163
25. Bernardi DM, Verbrugge MW (1992) A Mathematical model of the solid-polymer-electrolyte fuel cell. J Electrochem Soc 139:2477
26. Springer TE, Zawodzinski TA, Gottesfeld S (1991) Polymer electrolyte fuel cell model. J Electrochem Soc 138(8):2334–2342
27. He W, Yi JS, Van Nguyen T (2000) Two-phase flow model of the cathode of PEM fuel cells using interdigitated flow fields. AIChE J 46(10):2053–2064
28. Natarajan D, Van Nguyen T (2001) A two-dimensional, two-phase, multicomponent, transient model for the cathode of a proton exchange membrane fuel cell using conventional gas distributors. J Electrochem Soc 148:A1324
29. Nguyen TV, White RE (1993) A water and heat management model for proton-exchange-membrane fuel cells. J Electrochem Soc 140:2178

30. Wang ZH, Wang CY, Chen KS (2001) Two-phase flow and transport in the air cathode of proton exchange membrane fuel cells. J Power Sources 94(1):40–50
31. Nguyen PT, Berning T, Djilali N (2004) Computational model of a PEM fuel cell with serpentine gas flow channels. J Power Sources 130(1–2):149–157
32. Natarajan D, Van Nguyen T (2003) Three-dimensional effects of liquid water flooding in the cathode of a PEM fuel cell. J Power Sources 115(1):66–80
33. Bernardi DM (1990) Water-balance calculations for solid-polymer-electrolyte fuel cells. J Electrochem Soc 137:3344
34. Fuller TF, Newman J (1993) Water and thermal management in solid-polymer-electrolyte fuel cells. J Electrochem Soc 140:1218
35. Wohr M, Bolwin K, Schnurnberger W, Fischer M, Neubrand W, Eigenberger G (1998) Dynamic modelling and simulation of a polymer membrane fuel cell including mass transport limitation. Int J Hydrogen Energy 23(3):213–218
36. Barsoukov En, Macdonald JR (2005) Impedance spectroscopy: theory, experiment, and applications. Wiley, Hoboken, New Jersey, USA
37. Andreaus B, McEvoy AJ, Scherer GG (2002) Analysis of performance losses in polymer electrolyte fuel cells at high current densities by impedance spectroscopy. Electrochimica Acta 47(13–14):2223–2229
38. Ciureanu M, Mikhailenko SD, Kaliaguine S (2003) PEM fuel cells as membrane reactors: kinetic analysis by impedance spectroscopy. Catal Today 82(1–4):195–206
39. Macdonald DD (2006) Reflections on the history of electrochemical impedance spectroscopy. Electrochimica Acta 51(8–9):1376–1388
40. Primucci M, Ferrer L, Serra M, Riera J (2008) Characterisation of fuel cell state using Electrochemical Impedance Spectroscopy analysis. Simposium Ibérico de Hidrógeno, Pilas de Combustible y Baterías Avanzadas (HYCELTEC)
41. Alejandro J, Real D, Arce A, Bordons C (2007) Development and experimental validation of a pem fuel cell dynamic model. J Power Sources 173(1):310–324
42. Pathapati PR, Xue X, Tang J (2005) A new dynamic model for predicting transient phenomena in a pem fuel cell system. Renew Energy 30(1):1–22
43. El-Sharkh M, Rahman A, Alam M, Byrne P, Sakla A, Thomas T (2004) A dynamic model for a stand-alone PEM fuel cell power plant for residential applications. J Power Sources 138:199–204
44. An improved dynamic voltage model of pem fuel cell stack (2010) Int J Hydrogen Energy 35(20):11154–11160 Hyceltec 2009 Conference
45. Grujicic M, Chittajallu KM, Law EH, Pukrushpan JT (2004) Model-based control strategies in the dynamic interaction of air supply and fuel cell. Proc Inst Mech Eng, Part A: J Power Energy 218(7):487–499
46. Vahidi A, Peng A (2004) Model predictive control for starvation prevention in a hybrid fuel cell system. Am Control Conf, Proc 2004 1:834–839
47. Varigonda S, Pukrushpan JT, Stefanopoulou AG (2003) American Institute of Chemical Engineers. Challenges in fuel cell power plant control: the role of system level dynamic models. Am Inst Chem Eng 1:101–110
48. Gelfi S, Stefanopoulou AG, Pukrushpan JT, Huei Peng (2003) Dynamics of low-pressure and high-pressure fuel cell air supply systems. In: Am Control Conf, 2003. Proceedings of the 2003 3:2049–2054
49. Caux S, Lachaize J, Fadel M, Shott P, Nicod L (2005) Energy management of fuel cell system and supercaps elements. In: Proceedings of the 16th IFAC World Congress, Prague
50. Serra M, Aguado J, Ansade X, Riera J (2005) Controllability analysis of decentralized linear controllers for polymeric fuel cells. J Power Sources 151:93–102
51. Feroldi D, Serra M, Riera J (2007) Performance improvement of a pemfc system controlling the cathode outlet air flow. J Power Sources 169(1):205–212
52. Zenith F, Skogestad S (2007) Control of fuel cell power output. J Process Control 17(4):333–347

53. Ceraolo M, Miulli C, Pozio A (2003) Modelling static and dynamic behaviour of proton exchange membrane fuel cells on the basis of electro-chemical description. J Power Sources 113(1):131–144
54. Yang W, Bates B, Fletcher N, Pow R (1998) Control challenges and methodologies in fuel cell vehicles development. Fuel Cell Technol for Vehicles 1:249–256
55. Friedman D (1999) Maximizing direct-hydrogen PEM fuel cell vehicle efficiency-is hybridization necessary? SAE Int 1:265–272

http://www.springer.com/978-1-84996-183-7

PEM Fuel Cells with Bio-Ethanol Processor Systems
A Multidisciplinary Study of Modelling, Simulation, Fault Diagnosis and Advanced Control
Basualdo, M.S.; Feroldi, D.; Outbib, R. (Eds.)
2012, XXX, 462 p., Hardcover
ISBN: 978-1-84996-183-7